

Interchange between coordinated and lattice solvents generates the highest energy barrier within nine-coordinated Dy^{III} single molecule magnets

Lin Sun,^a Sheng Zhang,^{a,c} Zhijie Zhang,^a Qi Yang,^a Sanping Chen,^{*a} Yiquan Zhang,^{*b} Wenyuan Wang,^a Qing Wei,^a Gang Xie^a

^a Key Laboratory of Synthetic and Natural Functional Molecule Chemistry of Ministry of Education, College of Chemistry and Materials Science, Northwest University, Xi'an, Shaanxi 710127, China.

^b Jiangsu Key Laboratory for NSLSCS, School of Physical Science and Technology, Nanjing Normal University, Nanjing 210023, China

^c College of Chemistry and Chemical Engineering, Baoji University of Arts and Sciences, Baoji 721013, China.

Contents

Page S2 Single Crystal X-Ray Diffraction

Page S3 Thermogravimetric analysis

Page S3 X-Ray Powder Diffraction

Page S4 Crystal Structure

Page S6 Magnetic Measurements

Page S10 Results of *ab initio* investigation

Page S13 References

Single Crystal X-Ray Diffraction

Table S1. Crystallographic Data for compounds **1** and **2**.

Compound	1	2
Empirical formula	C ₁₄ H ₂₀ DyN ₇ O ₁₀	C ₁₆ H ₂₄ DyN ₇ O ₁₀
Formula weight	608.87	636.92
Temperature	296 K	296 K
Crystal system	Triclinic	Monoclinic
space group	<i>P</i> -1	<i>P</i> 2 ₁ /c
<i>a</i> (Å)	7.653(2)	10.892(4)
<i>b</i> (Å)	10.785(3)	24.650(9)
<i>c</i> (Å)	13.375(4)	9.988(3)
α (°)	90.525(5)	90
β (°)	92.108(4)	94.966(7)
γ (°)	104.345(5)	90
<i>V</i> (Å ³)	1068.6(5)	2671.7(16)
<i>Z</i>	2	4
<i>F</i> (000)	598	1260
Goodness-of-fit on <i>F</i> ²	1.050	1.110
Final <i>R</i> indices [<i>I</i> >2sigma(<i>I</i>)]	<i>R</i> 1 = 0.0433 <i>wR</i> 2 = 0.1098	<i>R</i> 1 = 0.0968 <i>wR</i> 2 = 0.1925
<i>R</i> indices (all data)	<i>R</i> 1 = 0.0526 <i>wR</i> 2 = 0.1232	<i>R</i> 1 = 0.1928 <i>wR</i> 2 = 0.2276
CCDC	1552858	1552859

Table S2. Selected bond lengths (Å) and angles (°) for **1** and **2**.

1					
Dy(1)-O(7)	2.319(5)	O(7)-Dy(1)-O(9)	148.18(19)	N(4)-Dy(1)-O(2)	75.35(18)
Dy(1)-O(8)	2.355(5)	O(9)-Dy(1)-O(4)	84.4(2)	O(8)-Dy(1)-O(2)	153.14(19)
Dy(1)-O(9)	2.376(5)	O(7)-Dy(1)-N(4)	65.26(18)	O(7)-Dy(1)-O(2)	80.61(18)
Dy(1)-N(4)	2.408(6)	O(7)-Dy(1)-O(4)	81.7(2)	O(8)-Dy(1)-O(4)	125.64(18)
Dy(1)-O(4)	2.437(6)	O(8)-Dy(1)-N(6)	84.90(18)	O(8)-Dy(1)-N(4)	78.00(18)
Dy(1)-O(2)	2.481(5)	O(7)-Dy(1)-N(6)	127.39(18)	O(1)-Dy(1)-N(6)	70.16(18)
Dy(1)-O(5)	2.496(5)	O(5)-Dy(1)-O(1)	115.04(19)	O(5)-Dy(1)-N(6)	150.21(19)
Dy(1)-O(1)	2.538(5)	O(2)-Dy(1)-O(1)	50.76(17)	O(2)-Dy(1)-N(6)	80.02(19)
Dy(1)-N(6)	2.607(6)	O(4)-Dy(1)-O(1)	70.09(19)	O(4)-Dy(1)-N(6)	140.0(2)
O(7)-Dy(1)-O(8)	91.31(17)	N(4)-Dy(1)-O(1)	112.60(18)	N(4)-Dy(1)-N(6)	62.63(19)
O(9)-Dy(1)-O(2)	124.35(18)	O(9)-Dy(1)-O(1)	73.61(18)	O(9)-Dy(1)-N(6)	80.16(19)
N(4)-Dy(1)-O(4)	140.6(2)	O(8)-Dy(1)-O(1)	141.81(17)	N(4)-Dy(1)-O(5)	130.1(2)
O(8)-Dy(1)-O(9)	73.97(18)	O(4)-Dy(1)-O(5)	52.0(2)	O(9)-Dy(1)-O(5)	74.0(2)
O(9)-Dy(1)-N(4)	134.9(2)	O(7)-Dy(1)-O(1)	126.76(17)	O(8)-Dy(1)-O(5)	74.03(18)

O(2)-Dy(1)-O(5)	127.09(19)	O(4)-Dy(1)-O(2)	78.77(19)	O(7)-Dy(1)-O(5)	74.86(18)
2					
Dy(1)-O(1)	2.275(10)	O(8)-Dy(1)-O(9)	81.9(4)	O(2)-Dy(1)-O(6)	68.1(4)
Dy(1)-O(8)	2.372(11)	N(3)-Dy(1)-O(9)	140.0(4)	O(3)-Dy(1)-O(6)	69.4(5)
Dy(1)-N(3)	2.403(13)	O(1)-Dy(1)-O(2)	99.2(4)	O(1)-Dy(1)-O(5)	142.2(4)
Dy(1)-O(9)	2.408(12)	O(8)-Dy(1)-O(2)	153.2(4)	O(8)-Dy(1)-O(5)	73.6(4)
Dy(1)-O(2)	2.476(12)	N(3)-Dy(1)-O(2)	76.4(4)	N(3)-Dy(1)-O(5)	135.9(4)
Dy(1)-O(3)	2.479(12)	O(9)-Dy(1)-O(2)	124.8(4)	O(9)-Dy(1)-O(5)	70.5(4)
Dy(1)-O(6)	2.514(11)	O(1)-Dy(1)-O(3)	77.2(5)	O(2)-Dy(1)-O(5)	115.2(4)
Dy(1)-O(5)	2.538(12)	O(8)-Dy(1)-O(3)	152.1(4)	O(3)-Dy(1)-O(5)	111.7(4)
Dy(1)-N(5)	2.601(14)	N(3)-Dy(1)-O(3)	108.0(5)	O(6)-Dy(1)-O(5)	50.1(4)
Dy(1)-N(6)	2.888(16)	O(9)-Dy(1)-O(3)	74.8(4)	O(1)-Dy(1)-N(5)	128.5(4)
O(1)-Dy(1)-O(8)	82.8(4)	O(2)-Dy(1)-O(3)	144.9(5)	O(8)-Dy(1)-N(5)	87.1(5)
O(1)-Dy(1)-N(3)	65.2(4)	O(1)-Dy(1)-O(6)	123.5(4)	N(3)-Dy(1)-N(5)	63.3(4)
O(8)-Dy(1)-N(3)	80.4(5)	N(3)-Dy(1)-O(6)	135.5(4)	O(9)-Dy(1)-N(5)	150.5(4)
O(1)-Dy(1)-O(9)	77.2(4)	O(9)-Dy(1)-O(6)	83.7(4)	O(2)-Dy(1)-N(5)	70.6(5)
O(3)-Dy(1)-N(5)	120.7(4)	O(6)-Dy(1)-N(5)	79.8(4)	O(5)-Dy(1)-N(5)	80.1(4)
O(1)-Dy(1)-N(6)	90.2(4)	O(8)-Dy(1)-N(6)	172.5(4)	N(3)-Dy(1)-N(6)	94.2(5)
O(9)-Dy(1)-N(6)	99.4(4)	O(2)-Dy(1)-N(6)	25.7(4)	O(3)-Dy(1)-N(6)	25.8(4)
O(6)-Dy(1)-N(6)	63.9(4)	O(5)-Dy(1)-N(6)	113.8(4)	N(5)-Dy(1)-N(6)	95.1(5)

Thermogravimetric analysis

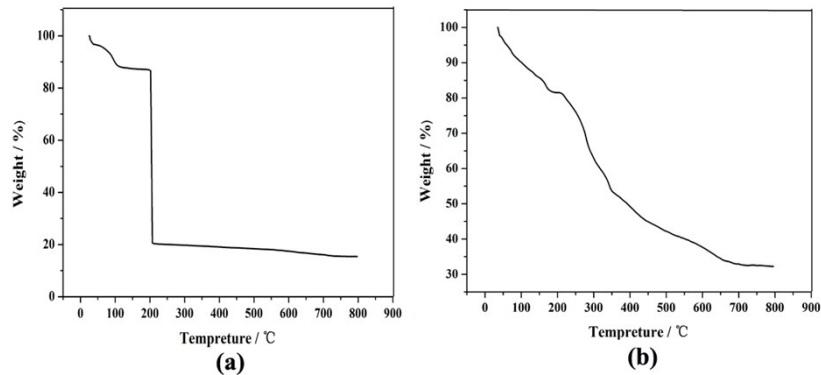


Figure S1. TGA curves of **1** and **2** under dry N_2 atmosphere. (left for **1** and right for **2**)

X-Ray Powder Diffraction

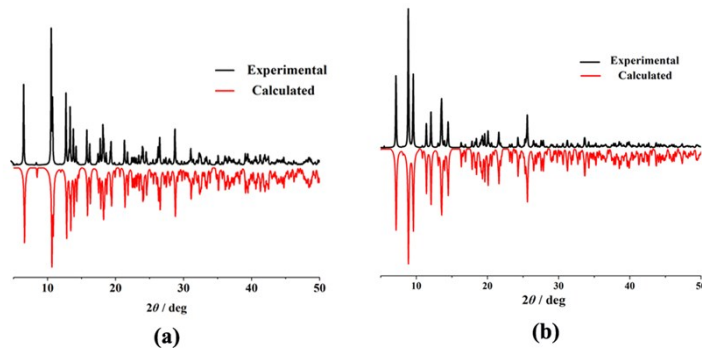


Figure S2. Experimental PXRD and calculated PXRD for **1** and **2**. (left for **1** and right for **2**)

Crystal Structure

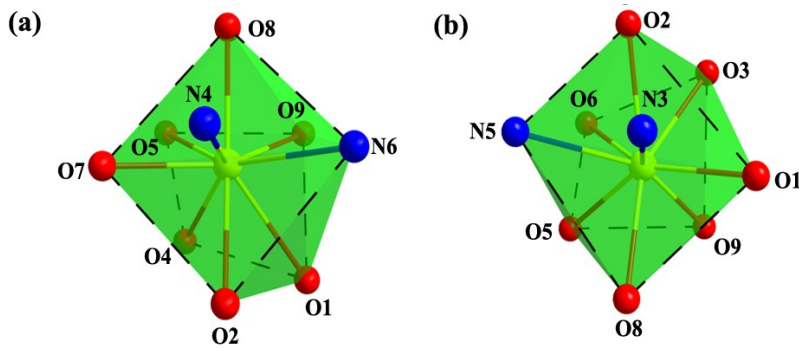


Figure S3. Local coordination geometry of the Dy^{III} ion in **1(a)** and **2(b)**.

Table S3. The calculated results for Dy^{III} ions configuration of **1–3** by SHAPE 2.1 software.

Configuration	ABOXIY, 1	ABOXIY, 3
Enneagon (D_{9h})	33.308	35.150
Octagonal pyramid (C_{8v})	22.854	23.774
Heptagonal bipyramid (D_{7h})	16.810	19.173
Johnson Triangular cupola J3 (C_{3v})	13.258	15.318
Capped Cube J8 (C_{4v})	9.071	10.811
Spherical-relaxed capped Cube (C_{4v})	7.687	9.434
Capped square antiprism J10 (C_{4v})	3.410	2.974
Spherical capped square antiprism (C_{4v})	2.332	1.819
Tricapped trigonal prism J51 (D_{3h})	2.874	3.925
Spherical tricapped trigonal prism (D_{3h})	2.132	2.446
Tridiminished icosahedron J63 (C_{3v})	11.671	10.004
Hula-hoop (C_{2v})	10.790	10.053

Packing diagrams for compounds **1** and **2**

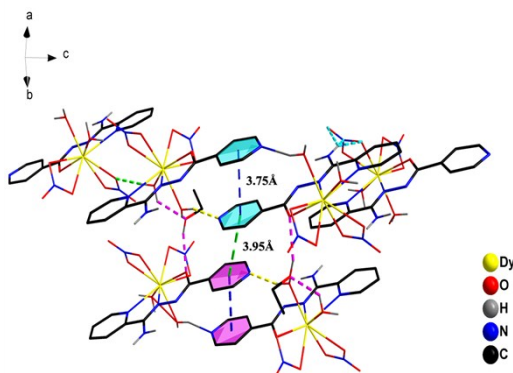
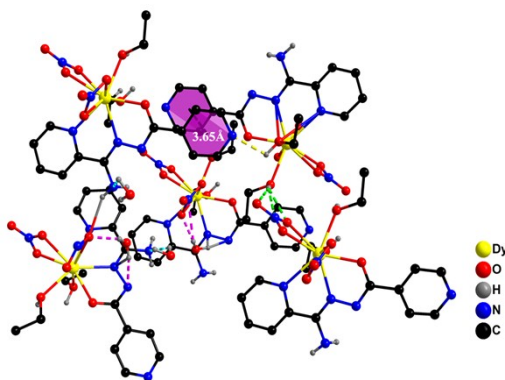


Figure S4. Packing diagram for compound **1**. The dotted lines represent the $\pi \cdots \pi$ interactions and the hydrogen bonding interactions.

Table S4. Hydrogen bond geometry in compound **1**.

D-H···A	$d_{D-H}/\text{\AA}$	$d_{H\cdots A}/\text{\AA}$	$d_{D\cdots A}/\text{\AA}$	$\angle \text{DHA}^\circ$
O(10)-H(10A)···O(7) ⁱ	0.82	2.07	2.846(7)	156.8
N(5)-H(5B)···N(1) ⁱⁱⁱ	0.86	2.66	3.264(9)	127.9
N(5)-H(5B)···O(3) ⁱⁱⁱ	0.86	2.49	2.997(9)	118.4
N(5)-H(5B)···O(2) ⁱⁱⁱ	0.86	2.44	3.178(9)	144.7
O(9)-H(9B)···O(10)	0.85	2.12	2.750(8)	129.9
O(9)-H(9A)···O(1) ⁱⁱ	0.85	2.04	2.817(7)	150.8
O(8)-H(8B)···N(7) ^{iv}	0.79	1.94	2.684(8)	158.3
O(8)-H(8A)···O(10)	0.97	1.80	2.748(7)	163.0

(i) x-1,y,z; (ii) -x+1,-y,-z; (iii) -x+2,-y+1,-z; (iv) -x+2,-y+1,-z+1.

**Figure S5.** Packing diagram for compound **2**. The dotted lines represent the $\pi\cdots\pi$ interactions and the hydrogen bonding interactions.**Table S5.** Hydrogen bond geometry in compound **2**.

D-H···A	$d_{D-H}/\text{\AA}$	$d_{H\cdots A}/\text{\AA}$	$d_{D\cdots A}/\text{\AA}$	$\angle \text{DHA}^\circ$
O(11)-H(11B)…N(4)	0.90	2.55	3.302(5)	141.6
N(4)-H(4B)…O(2) ⁱⁱⁱ	0.89	2.22	2.963(18)	140.6
O(9)-H(9)…N(7) ^{iv}	0.97	2.64	3.53(2)	152.7
O(9)-H(9)…O(7) ^{iv}	0.97	2.34	3.30(2)	166.7
O(9)-H(9)…O(5) ^{iv}	0.97	2.30	2.951(16)	123.5
O(8)-H(8)…N(1) ^v	0.97	2.15	2.634(19)	109.3

(i) x+1,y,z+1; (ii) -x+2,-y,-z+1; (iii) x,-y+1/2,z+1/2; (iv) -x+1,-y,-z+1; (v) -x+2,-y,-z+2.

Magnetic Measurements

The fit of the experimental χ_M data to the Curie–Weiss law in the temperature range of 300–2 K results in the Curie constant ($C = 12.59 \text{ cm}^3 \text{K mol}^{-1}$ for **1**, $C = 14.55 \text{ cm}^3 \text{K mol}^{-1}$ for **2**) and a small Weiss temperature ($\theta = -2.69 \text{ K}$ for **1**, $\theta = -0.99 \text{ K}$ for **2**) suggesting very weak antiferromagnetic interactions overall for **1** and **2**.

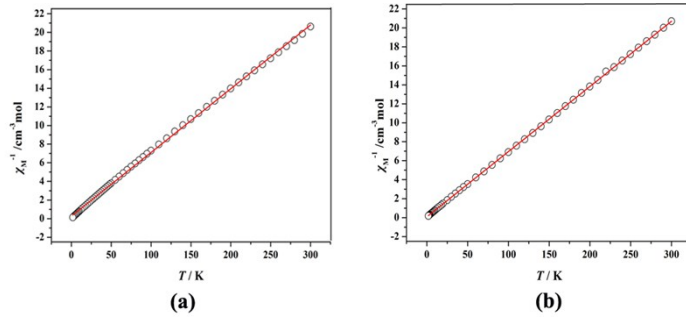


Figure S6. $1/\chi_M$ versus T plots with Curie–Weiss fitting as the red lines ($C = 12.59 \text{ cm}^3 \text{K mol}^{-1}$; $\theta = -2.69 \text{ K}$ and $C = 14.55 \text{ cm}^3 \text{K mol}^{-1}$; $\theta = -0.99 \text{ K}$) for **1** and **2**, respectively.

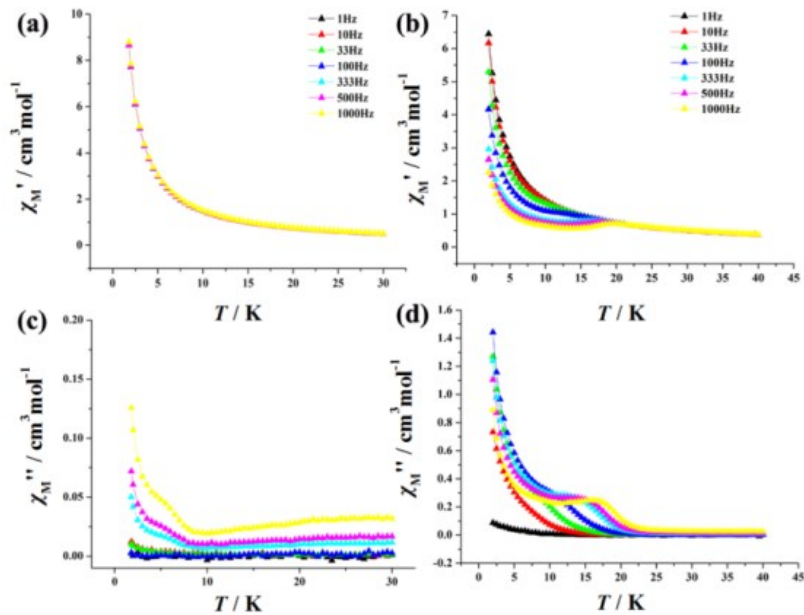


Figure S7. Temperature dependence of the in-phase (a and c) and out-of phase (b and d) ac susceptibility signals under 0 Oe dc field for **1** and **2**, respectively.

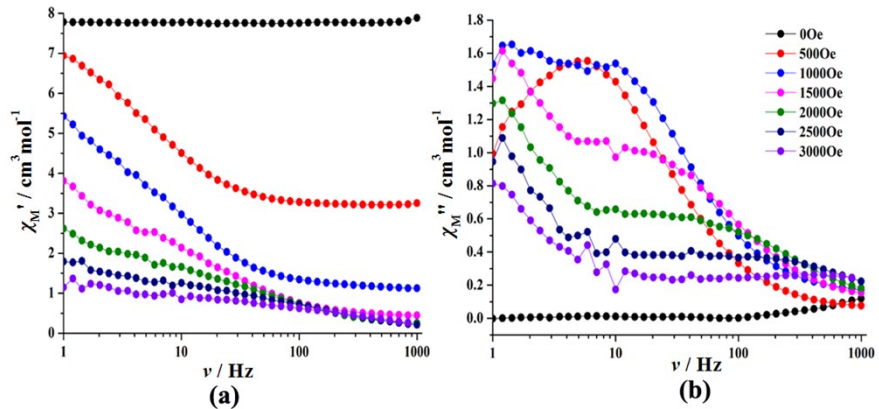


Figure S8. Imaginary susceptibility of **1** at 2.0 K as a function of the applied field.

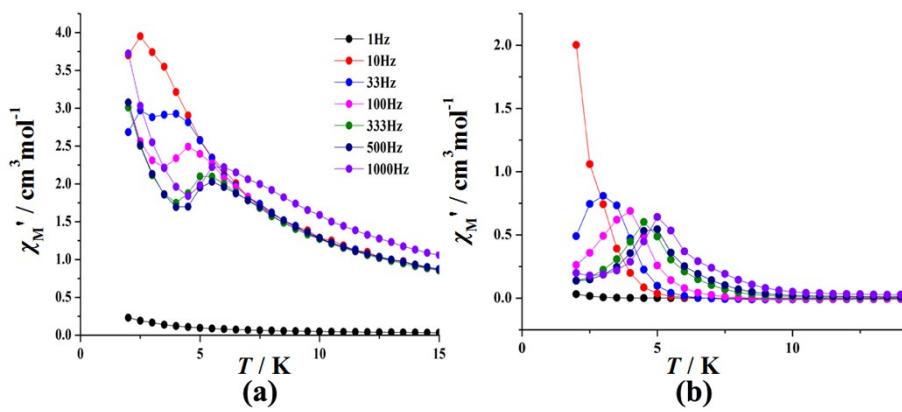


Figure S9. Plots of the frequency-dependent in-phase (a) and out-of-phase (b) ac susceptibility for **1** at indicated temperatures under 500 Oe dc field.

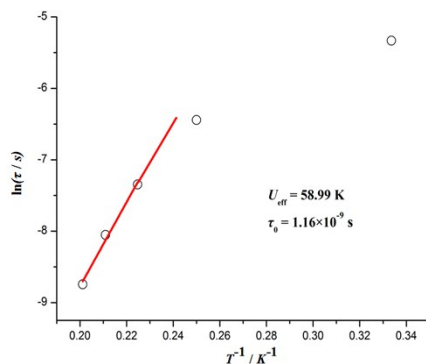


Figure S10. Magnetic relaxation time $\ln\tau$ versus T^{-1} plots with linear fits of the thermally activated region (d) for **1** under 500 Oe dc field.

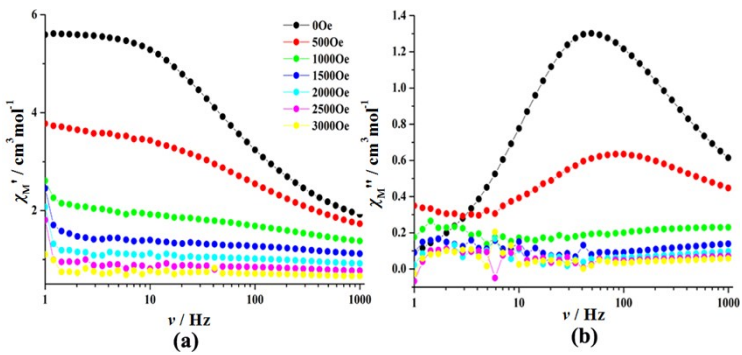


Figure S11. Imaginary susceptibility of **2** at 2.0 K as a function of the applied field.

Table S6. Relaxation fitting parameters from Least-Squares Fitting of $\chi(\omega)$ data of **2**.

T(K)	$\Delta\chi_1$ ($\text{cm}^3\text{mol}^{-1}$)	$\Delta\chi_2$ ($\text{cm}^3\text{mol}^{-1}$)	A
2.0	5.44602	1.96200	0.26562
3.0	3.81094	1.78438	0.29487
4.0	2.92062	0.93823	0.28579
5.0	2.36229	0.78109	0.27183
6.0	1.98457	0.66421	0.26576
7.0	1.75782	0.53609	0.31964
8.0	1.55992	0.4848	0.31838
9.0	1.38505	0.47308	0.28364
10.0	1.25333	0.45937	0.25438
11.0	1.03782	0.41885	0.01674
12.0	0.95147	0.42841	0.08259
12.5	0.9183	0.41335	0.07956
13.0	0.8849	0.42354	0.03282
13.5	0.85686	0.41117	0.02800
14.0	0.83025	0.39843	0.02232
15.0	0.8060	0.38389	0.01980
15.5	0.80593	0.38285	0.02060
16.0	0.78266	0.36074	0.02561
16.5	0.76195	0.31296	0.05620

The detail on fitting for 2: Considering three parameters, the fitting may be not accurate. Firstly, a linear fitting of the thermally activated points to the Arrhenius law ($\tau = \tau_0 \exp(U_{\text{eff}}/kT)$) afford $U_{\text{eff}} = 172.12$ K (119.62 cm $^{-1}$) and $\tau_0 = 1.52 \times 10^{-7}$ s at high temperature regime (13.5–16.5K). Subsequently, transitioning over to non-linear regime at middle temperature regime (13.5–5.0 K), but not becoming temperature independent, fiting the data (16.5–5.0 K) by thermally activated Orbach and Raman processes ($\tau = CT^n + \tau_0^{-1} \exp(-U_{\text{eff}}/kT)$) gives $U_{\text{eff}} = 253.44$ K (176.14 cm $^{-1}$), $\tau_0 = 8.87 \times 10^{-11}$ s, $C = 12.86$ s $^{-1}$ K $^{-n}$, $n = 2.02$. Finally, the fit in the temperature range $T = 2.0$ –16.5 K by eqn (1) resulted in $\tau_{\text{QTM}} = 0.00295$ s, $n = 2.59$, $C = 2.33$ s $^{-1}$ K $^{-5}$, $\tau_0 = 1.77 \times 10^{-9}$ s, and an effective energy barrier of $U_{\text{eff}} = 203.11$ K (141.16 cm $^{-1}$) (Figure 4d).

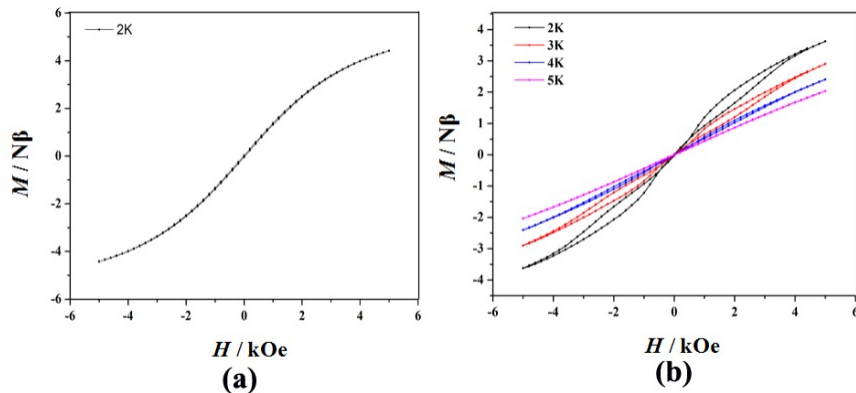


Figure S12. Normalized magnetic hysteresis loops for **1** (a) and **2** (b).

Results of *ab initio* investigation

Complete-active-space self-consistent field (CASSCF) calculations on the complete structures (see Figure S14 for the complete structures of **1** and **2**) of compounds **1–2** on the basis of X-ray determined geometry have been carried out with MOLCAS 8.0 program package.^[S1]

For CASSCF calculation, the basis sets for all atoms are atomic natural orbitals from the MOLCAS ANO-RCC library: ANO-RCC-VTZP for Dy^{III} ion; VTZ for close N and O; VDZ for distant atoms. The calculations employed the second order Douglas-Kroll-Hess Hamiltonian, where scalar relativistic contractions were taken into account in the basis set and the spin-orbit coupling was handled separately in the restricted active space state interaction (RASSI-SO) procedure. The active electrons in 7 active spaces include all *f* electrons (CAS (9 in 7) for complexes **1–2**) in the CASSCF calculation. To exclude all the doubts we calculated all the roots in the active space. We have mixed the maximum number of spin-free state which was possible with our hardware (all from 21 sextets, 128 from 224 quadruplets and 130 from 490 doublets).

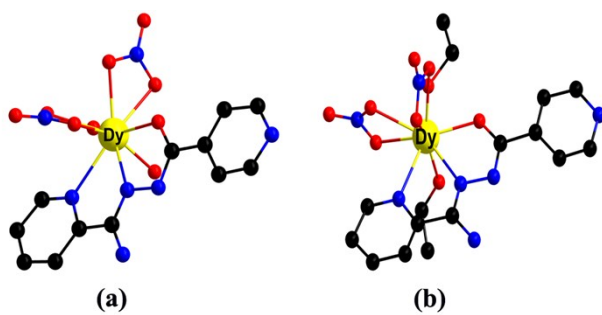


Figure S13. Calculated complete structure of compounds **1** and **2**; H atoms are omitted.

Table S6. Calculated energy levels (cm^{-1}), \mathbf{g} (g_x , g_y , g_z) tensors and m_J values of the lowest Kramers doublets (KDs) of the Dy fragments of compounds **1–2**.

1				2					
KDs	E/cm^{-1}	\mathbf{g}		m_J	KDs	E/cm^{-1}	\mathbf{g}		m_J
1	0.0	g_x	0.208	$\pm 15/2$	1	0.0	g_x	0.001	$\pm 15/2$
		g_y	0.743				g_y	0.004	
		g_z	18.733				g_z	19.704	
2	49.7	g_x	0.101	$\pm 13/2$	2	211.9	g_x	0.445	$\pm 13/2$
		g_y	0.553				g_y	0.752	
		g_z	17.438				g_z	16.322	
3	166.7	g_x	2.942	$\pm 11/2$	3	269.9	g_x	0.276	$\pm 9/2$
		g_y	3.550				g_y	1.226	
		g_z	13.253				g_z	17.020	
4	209.1	g_x	8.785	$\pm 3/2$	4	316.7	g_x	2.077	$\pm 11/2$

		g_y	6.726				g_y	6.115	
		g_z	0.219				g_z	11.373	
5	267.4	g_x	8.401	$\pm 1/2$	5	346.0	g_x	1.559	$\pm 7/2$
		g_y	6.391				g_y	5.148	
		g_z	0.275				g_z	8.771	
6	304.4	g_x	1.104	$\pm 5/2$	6	379.6	g_x	1.163	$\pm 5/2$
		g_y	5.801				g_y	3.612	
		g_z	10.728				g_z	11.499	
7	349.1	g_x	1.059	$\pm 9/2$	7	438.9	g_x	0.656	$\pm 3/2$
		g_y	2.978				g_y	1.061	
		g_z	12.893				g_z	15.833	
8	725.5	g_x	0.873	$\pm 7/2$	8	503.7	g_x	0.282	$\pm 1/2$
		g_y	2.526				g_y	0.977	
		g_z	16.671				g_z	18.674	

Table S7. In wave functions with definite projection of the total moment $| JM \rangle$ for the lowest four Kramers doublets (KDs) of the Dy^{III} for compounds **1** and **2**.

	E/cm^{-1}	wave functions
1	0.0	85% $\pm 15/2$ >+7% $\pm 11/2$ >
	49.7	8% $\pm 15/2$ >+28% $\pm 13/2$ >+18% $\pm 11/2$ >+19% $\pm 9/2$ >+9% $\pm 7/2$ >+7% $\pm 5/2$ >+5% $\pm 3/2$ >+6% $\pm 1/2$ >
	166.7	42% $\pm 11/2$ >+13% $\pm 7/2$ >+9% $\pm 5/2$ >+13% $\pm 3/2$ >+12% $\pm 1/2$ >
	209.1	16% $\pm 13/2$ >+15% $\pm 11/2$ >+18% $\pm 9/2$ >+10% $\pm 7/2$ >+21% $\pm 5/2$ >+13% $\pm 3/2$ >+6% $\pm 1/2$ >
2	0.0	97% $\pm 15/2$ >
	211.9	74% $\pm 13/2$ >+6% $\pm 11/2$ >+16% $\pm 9/2$ >
	269.9	19% $\pm 11/2$ >+9% $\pm 9/2$ >+34% $\pm 7/2$ >+22% $\pm 5/2$ >+10% $\pm 3/2$ >
	269.9	15 $\pm 13/2$ >+33% $\pm 11/2$ >+28% $\pm 9/2$ >+7% $\pm 5/2$ >+7% $\pm 3/2$ >+5% $\pm 1/2$ >

Table S8. Natural Bond Order (NBO) charges per atoms in the ground state of compounds **1** and **2** calculated within CASSCF.

Atom	1	Atom	2
Dy	2.519	Dy	2.516
O3	-0.710	O8	-0.627
O1	-0.722	O9	-0.631
O4	-0.646	O3	-0.666
O5	-0.666	O2	-0.637
O7	-0.814	O1	-0.843
O8	-0.616	O6	-0.597
O2	-0.675	O5	-0.718
N2	-0.410	N3	-0.343
N1	-0.364	N5	-0.365

Table S9. *Ab Initio* Computed Crystal-Field Parameters for Compounds **1** and **2**.^a

k	q	B(k,q)	
		1	2
2	-2	0.1857	-0.8310
2	-1	0.1451 × 10¹	0.3840
2	0	-0.3123 × 10¹	-0.2084 × 10¹
2	1	0.7286	-0.2293
2	2	0.2218 × 10¹	0.6228
4	-4	-0.2386 × 10 ⁻³	0.2840 × 10 ⁻²
4	-3	-0.2584 × 10 ⁻¹	0.1353 × 10 ⁻¹
4	-2	0.2520 × 10 ⁻¹	-0.2926 × 10 ⁻²
4	-1	-0.3744 × 10 ⁻²	0.1293 × 10 ⁻¹
4	0	-0.6926 × 10 ⁻²	-0.3110 × 10 ⁻²
4	1	-0.1062 × 10 ⁻¹	-0.1740 × 10 ⁻³
4	2	-0.7110 × 10 ⁻²	0.1155 × 10 ⁻¹
4	3	-0.4883 × 10 ⁻¹	-0.1277 × 10 ⁻²
4	4	-0.7736 × 10 ⁻²	-0.1744 × 10 ⁻¹
6	-6	0.8775 × 10 ⁻⁴	0.9816 × 10 ⁻⁴
6	-5	-0.4735 × 10 ⁻³	0.1820 × 10 ⁻³
6	-4	-0.4785 × 10 ⁻⁴	-0.5592 × 10 ⁻⁴
6	-3	0.1177 × 10 ⁻³	-0.6512 × 10 ⁻⁴
6	-2	-0.6658 × 10 ⁻⁴	-0.5087 × 10 ⁻⁴
6	-1	-0.3691 × 10 ⁻⁴	-0.2479 × 10 ⁻³
6	0	0.4875 × 10 ⁻⁵	-0.3266 × 10 ⁻⁴
6	1	0.1233 × 10 ⁻³	-0.2564 × 10 ⁻⁴
6	2	0.1847 × 10 ⁻⁴	0.5277 × 10 ⁻⁴
6	3	-0.3021 × 10 ⁻³	-0.2561 × 10 ⁻³
6	4	-0.6423 × 10 ⁻⁴	-0.5461 × 10 ⁻⁵
6	5	0.1923 × 10 ⁻³	0.2254 × 10 ⁻⁴
6	6	0.7829 × 10 ⁻⁴	-0.2010 × 10 ⁻³

^aOnly the ranks k= 2, 4, and 6 are shown; higher ranks are much smaller and are not shown here.

Reference

S1 G. Karlström, R. Lindh, P. Å. Malmqvist, B. O. Roos, U. Ryde, V. Veryazov, P. O. Widmark, M. Cossi, B. Schimmelpfennig, P. Neogrády, L. Seijo, *Comput. Mater. Sci.*, 2003, **28**, 222–239.